Improved Short Time Thermal Transient Model and Testing Procedure for High Power Density Motors

Improved Short Time Thermal Transient Model and Testing Procedure for High Power Density Motors

Paolo Pescetto
Energy department Galileo Ferraris
Politecnico di Torino
Torino, Italy
paolo.pescetto@polito.it

Gaetano Dilevrano
Energy department Galileo Ferraris
Politecnico di Torino
Torino, Italy
gaetano.dilevrano@polito.it

Gianmario Pellegrino
Energy department Galileo Ferraris
Politecnico di Torino
Torino, Italy
gianmario.pellegrino@polito.it

Aldo Boglietti
Energy department Galileo Ferraris
Politecnico di Torino
Torino, Italy
aldo.boglietti@polito.it

***Abstract*—The Short Time Thermal Transient (STTT) testing procedure is a fast and accurate method for evaluating the winding thermal capacitance and winding to back iron thermal resistance of AC motors. This procedure has been extensively validated for industrial motors and involves short duration DC excitation with the motor phases connected in series, followed by data analysis based on a first-order lumped parameter thermal network. However, when the phase terminals are not fully accessible, such as in motor drives for traction, the all-in-series canonical STTT procedure cannot be used. Additionally, for highly loaded traction motors, the estimated thermal parameters are more dependent on the duration of the DC excitation, rendering the existing first-order STTT model impractical. To address these issues, this paper presents and improved STTT model, the related testing sequence and data processing approach having a wider and more general, to be used in a wider range of applications. The new approach is validated through experimental results.**

***Index Terms*—Short time thermal transient, Thermal Network, Traction motor drives, Thermal testing, Temperature observer, Hot spot winding temperature, Thermal Management.**

I. Introduction

The cost, weight and volume effective design of high performance electric machines requires a multi-physics approach [1], with the magnetic design complemented within the mechanical and thermal domains [2]–[4]. This need is today emphasized by the increasingly demanding cost and performance requirements dictated by the automotive industry for traction electric motors [5]–[7]. The increasing power density requirements demand for better thermal management, and liquid cooled motors for traction have minimized thermal impedance and short thermal time constants. Accordingly, the testing of electric motors is not only related to their magnetic characteristics [8], [9], but reliable procedures for experimentally determining the machine's thermal properties have become essential [10].

Accurate thermal models are necessary at both the design and control stages for advanced thermal management of electric machines [12], [13]. Such models are either based on Finite Element Analysis (FEA) or Lumped Parameters Thermal Networks (LPTNs) [14], or both. While FEA provides greater accuracy, it requires detailed information about the geometry and thermal properties of each motor component, which may not be readily available to the end users. In contrast, LPTNs offer a less detailed but still accurate estimation of temperature for different parts of the motor, with minimal computational effort. Thus, we adopt and develop the LPTN approach in this work.

An accurate LTPN model must include the key parts of the motor, such as rotor and stator iron, windings, Permanent Magnets (PM). Among these parts, the winding is a vulnerable component due to its strict isolation class temperature limit, especially when liquid cooling is used and hot-spot thermal transients become relatively fast. The thermal coupling between the winding conductors and the surrounding insulation material and stator iron is difficult to compute analytically or numerically [15]–[17]. Therefore, the Short Time Thermal Transient (STTT) test procedure was introduced [11], [18] for direct experimental evaluation of the winding thermal capacitance and resistance, referring to a 1st order model and general purpose induction motors with all the windings terminals accessible. This paper shows that the STTT method can fail describing the transient behavior of high machines with liquid cooling and low thermal inertia [19], [20]. In fact, the original STTT procedure assumes that the winding-to-iron thermal time constant is much faster than the iron-to-ambient heat exchange temperature effect, which does not hold true for the liquid cooled motors under investigation. As a result, the STTT-derived winding thermal capacitance and resistance are highly dependent on the test's duration and selected temperature STTT temperature rise.

This paper improves the STTT model and data processing procedure of [11], and presents experimentally validated results using a star-connected traction motor with the three phase input terminals and a weak connection to the star point

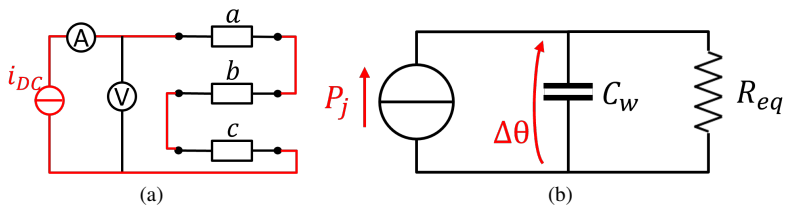

Fig. 1. Existing STTT procedure [11]. (a) DC identification test. (b) Equivalent LPTN.

accessible. The improved model overcomes the limitations of [11] by admitting the temperature variation of the back iron during the STTT test. Thanks to the proposed analysis, the dependency of the estimated thermal parameters on the test duration is reduced by one order of magnitude.

II. Motor under test

The machine adopted for validating the proposal is a Permanent Magnet Synchronous Motor (PMSM) for high performance traction applications. As common for traction motors, the phase resistance is in the order of a few $m\Omega$. In the embarkable version, only the input terminals of the three phases are accessible, which makes the existing STTT procedure [11] unfeasible. In the prototype under test, an additional wire of reduced cross-section permits to access the winding star point with limited current capability and a resistance comparable to the phase resistance.

Although not required for the STTT, the motor encapsulates seven thermistors for mapping the thermal gradient inside the machine. It should be noted that the design of this machine is proprietary, so every physical quantity in the paper is normalized. The nominal thermal capacitance of the winding and thermal resistance resistance are defined based on the finite element model of the machine, while the rated temperature rise is defined as the difference between the maximum allowed winding temperature and the nominal ambient temperature during operation.

III. Existing 1st Order STTT Procedure

The Short Time Thermal Transient (STTT) is a testing procedure meant for estimating the slot thermal parameters of three-phase [11] or multi-phase [18] electric motors. The winding thermal capacitance C_w, and the equivalent thermal resistance R_{eq} between the winding and the stator iron, including isolation and potting, are estimated by experiments.

In the testing procedure [11], the three phases are series connected, as in Fig. 1a. Starting from the motor at a uniform initial temperature θ_o, the series of the three phases is DC excited with a value of current compatible with the RMS nominal current, producing a measurable temperature rise. The series connection ensures that the three phases are heated evenly. The imposed current i_{dc} and the voltage v_{dc} across the series of the three phases are measured, computing the winding resistance R_{dc}, Joule loss P_j and average winding temperature θ:

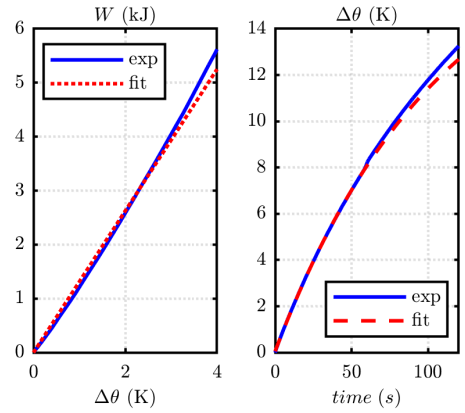

Fig. 2. Example of STTT test results for an industrial motor drive according to [11]. Left: dissipated energy as a function of the overtemperature; right: overtemperature as a function of time. Blue: measured data; red: interpolations with (4) and (5) respectively.

$$R_{dc} = \frac{v_{dc}}{3i_{dc}} \tag{1a}$$

$$P_j = v_{dc} \cdot i_{dc} \tag{1b}$$

$$\theta = \frac{R_{dc}}{R_o}(234.5 + \theta_o) - 234.5 \tag{1c}$$

where R_o is the winding resistance measured at θ_o. Under DC excitation, the input power coincides with the Joule loss in the windings. Therefore, the copper energy loss W can be computed as the time integral of P_j:

$$W = \int_{t_0}^{t} P_j \, dt \tag{2}$$

where t_0 is the time where the current step is imposed, and $W(t_0) = 0$.

The key assumption of the STTT procedure [11] is that in the initial short time horizon of the thermal transient the system is adiabatic, that is the heat exchange from the winding to the rest of the machine being negligible. This is reasonable as the heat is firstly generated into the copper winding, and just later it is dissipated mainly to the stator iron. The adiabatic hypothesis is valid for a minor initial temperature increase of the winding $\Delta\theta_{st}$

$$\Delta\theta = \theta - \theta_o < \Delta\theta_{st} \tag{3}$$

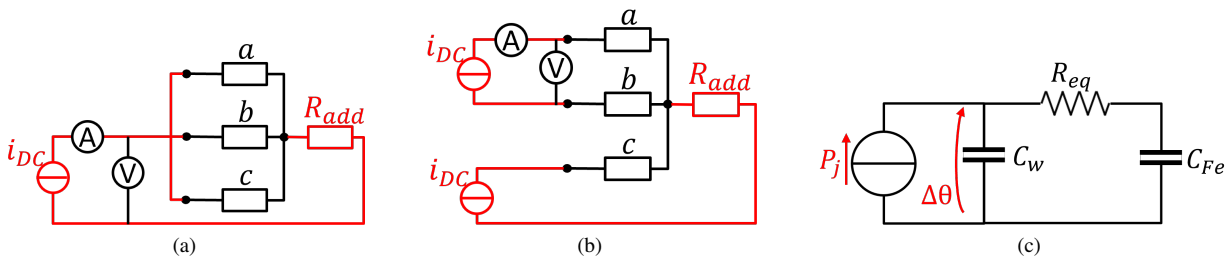

(a) (b) (c)

Fig. 3. Proposed STTT procedure. (a) Parallel DC identification. (b) Proposed DC identification. (c) Proposed LPTN.

where $\Delta\theta$ is the temperature rise with respect to the initial condition. Otherwise said, the initial heating of copper is considered adiabatic until the temperature rise reaches $\Delta\theta_{st}$, which is in the order of 3-5°C.

Under this assumption, the dissipated energy grows linearly with the winding temperature in the first instants of the transient, and the energy evolution $W(\Delta\theta)$ can be approximated with a straight line $\hat{W}(\Delta\theta)$, function of the temperature rise. The rate of change of the interpolating straight line provides an estimate of the winding thermal capacitance C_w:

$$\hat{W}\left(\Delta\theta\right) = a \cdot \Delta\theta \quad \rightarrow \quad C_w = a \tag{4}$$

The first order LPTN depicted in Fig. 1b represents the stator winding during the adiabatic STTT lapse, where the just determined C_w is "charged" by the Joule loss and the thermal resistance R_{eq} dissipates the heat to the surrouinding iron. As in the first part of the thermal transient the stator iron is assumed at constant θ_o, its thermal capacitance is omitted from the LPTN.

The parameter R_{eq} represents the aggregate thermal resistance between the stator copper and iron. R_{eq} is obtained by fitting the evolution of the winding temperature rise over time with the analytical solution of the LPTN. This second fitting is carried over the time domain $[0 \quad \Delta t_{st}]$, where Δt_{st} is the STTT time horizon:

$$\hat{\Delta\theta}\left(t\right) = P_j R_{eq}\left(1 - e^{-t/\tau_{eq}}\right) \quad \rightarrow \quad R_{eq} = \frac{\tau_{eq}}{C_w} \tag{5}$$

An example of STTT test on an industrial motor drive is reported in Fig. 2, where the procedure in [11] was adopted. The figure reports in blue the dissipated energy and overtemperature characteristics, and in red the interpolations using (4) and (5) respectively. As can be seen, for this type of motors the procedure in [11] is accurate, as the fitting functions well represent the measurements, so reliable values of C_w and R_{eq} can be extracted. Anyway, this test tends to fail for high preformance motors, as will be described in the next section.

IV. Proposed Identification and Data Processing

The motor under test presents several peculiarities making the traditional STTT procedure unfeasible (not all phase terminals are accessible) and unreliable (the 1st-order model fails). These issues have been solved in the present work, as described in this section.

A. Parallel Phase Connection

As said in Section III, series connection reported in Fig. 1a is not feasible in embarkable traction motors, where normally only the input terminals of the three phases are available. In the prototype under test the star point is made accessible through an additional connection having a resistance R_{add} compatible with the phase resistance, due to the small gauge of the additional wire.

A first alternative to the all-series connection is the parallel connection of Fig. 3a. This is still heating the three phases evenly, but with two downsides:

1) controlling a high direct current on a small resistance;
2) having the resistance R_{add} in series with the motor resistances.

About point 1, the DC current generator must provide three times the rated RMS phase current of the machine, which is already in the order of hundreds of A, to a load of a few $m\Omega$ or less, seen the paralleled phases. For example 300÷700 A at 1÷5 V. Controlling a stable and accurate direct current turns our to be a hard challenge for most of DC sources, and requires specialized equipment. Dealing with point 2, the term R_{add} is not related to the winding temperature and invalidates the winding temperature estimation through (1c). Considering these issues, the parallel connection in Fig. 3a has been dismissed.

The effect of R_{add} on the average temperature estimate is reported in Fig. 4, where the three phases were parallel connected and dc excited. The figure reports in black the average winding temperature, estimated with (1c), together with the measurements coming from all the thermistors embedded in the winding of the prototype, meant for mapping its thermal gradient, including the temperature hotspots. As can be see, the temperature estimate computed with (1c) is larger than any measured temperature, which is not realistic. This is explained considering that the additional wire adopted for accessing the star point, having a reduced section, was considerably hotter than the stator winding, thus deviating the average temperature estimate.

B. Proposed Dual Supply Connection

Alternatively to the parallel phase connection, two DC current sources were adopted as in Fig. 3b. The first DC source excites the phases a and b, and it is used for measuring the phase resistance, loss and temperature variation. The second

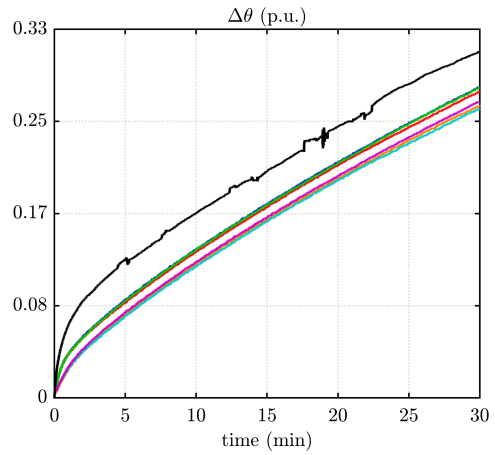

Fig. 4. Effect of R_{add} on the average winding temperature estimate (black line) under parallel phases connection, DC excitation. The colored lines refer to local winding temperatures measured with dedicated thermistors.

DC source excites the third phase through the star point with the exact same current, to maintain the thermal symmetry of the phases. This topology requires two DC sources with 1/3 of the current rating compared to the one of Fig. 3a. Moreover, the a to b measurement branch does not include R_{add}, permitting an independent estimation of the average winding temperature via (1c). The resistance and dissipated power computations are modified as:

$$R_{dc} = \frac{v_{dc}}{2i_{dc}} \tag{6a}$$

$$P_j = \frac{3}{2} v_{dc} \cdot i_{dc} \tag{6b}$$

The phase connection of Fig. 3b proved to be accurate and was adopted for the proposed STTT test.

C. Improved Model and Parameters Extraction

A crucial aspect of the original STTT in [11] is that the duration of the initial thermal transient, i.e. the adiabatic temperature rise range $\Delta\theta_{st}$ and the corresponding time interval Δt_{st} where the system follows a first order transient, was easy to be chosen arbitrarily. In practice, the temperature domain of interpolation of the dissipated energy with (4) and the time domain of interpolation of the temperature rise with (5) were easily determined by trial and error.

In this respect, the technique showed its robustness for industrial motors, fogiving even large temperature and time interval variations. Conversely, compact and highly-loaded traction machines are designed for an extremely high-rate of heat extraction. For this reason, the fundamental hypothesis of the STTT, i.e. that the initial part of the thermal transient is adiabatic, tends to fail. In particular the function $W(\Delta\theta)$ immediately starts growing non linearly, and cannot be approximated with a straight line to determine the thermal capacitance C_w with (4).

To solve this issue, a non-linear $W(\Delta\theta)$ function was considered, and approximated with its third-order Taylor series expansion.

$$\hat{W}\left(\Delta\theta\right) = a_3 \cdot \Delta\theta^3 + a_2 \cdot \Delta\theta^2 + a_1 \cdot \Delta\theta \tag{7}$$

The initial derivative of $W(\Delta\theta)$ still corresponds to the winding thermal capacitance C_w, and can be analytically determined as:

$$\left.\frac{d\hat{W}}{d\Delta\theta}\right|_{\Delta\theta=0} = a_1 \rightarrow \qquad C_w = a_1 \tag{8}$$

Additionally, the high thermal coupling between the stator winding and iron makes the original LPTN in Fig. 1b unreliable, as the heat transfer to the iron cannot be neglected. Also in this case, the estimation of R_{eq} through (5) would highly depend on the selected interpolation time Δt_{st}. This shortcoming was solved by including the iron thermal capacitance C_{Fe} in the equivalent LPTN, as shown in Fig. 3c. The heat dissipation from the stator iron to the coolant or to the ambient is not considered, as it is negligible in the initial thermal transient. Therefore, **the adiabatic assumption is moved from the winding alone to the stator altogether**. The temperature rise is again interpolated through the analytical solution of the LPTN, permitting to estimate the parameter R_{eq} from the time constant τ_{eq}:

$$\hat{\Delta\theta}\left(t\right) = \frac{P_j}{C_w + C_{Fe}} t + P_j R_{eq} \frac{C_{Fe}^2}{\left(C_w + C_{Fe}\right)^2} \left(1 - e^{-t/\tau'_{eq}}\right) \tag{9a}$$

$$\tau'_{eq} = \frac{C_w C_{Fe}}{C_w + C_{Fe}} \cdot R_{eq} \approx C_w \cdot R_{eq} \tag{9b}$$

V. Experimental Results

The proposed procedure was experimentally tested on the adopted traction motor. Fig. 5 depicts the test bench. Starting from uniform room temperature, the motor was excited according to Fig. 3b with a current of 0.5 p.u.. Although only the initial thermal transient is of interest for the STTT procedure, the DC excitation was maintained for a largely longer time, to evaluate the effect of $\Delta\theta_{st}$ and Δt_{st} calibration.

A. Parameters Identification

Fig. 6 reports in blue the experimentally measured energy variation Vs temperature rise, and the temperature rise Vs time curves. In Fig. 6a, data were interpolated as in [11] using (4) and (5), under different fitting domains, with $\Delta\theta_{st}$ spanning from 2 to 10 K and Δt_{st} from 10 to 200 s. As the estimate of C_w is the slope of the interpolating straight line (4), this strongly depends on the adopted $\Delta\theta_{st}$. Also, based on (5), the R_{eq} estimate derives from the time constant of the 1st order temperature rise fit, which again considerably varies with the choice of the time interval. This confirms that the existing

Fig. 5. Test bench for the experimental validation.

STTT procedure leads to unreliable estimation of the STTT parameters.

The same set of measurements was analyzed with the proposed procedure, i.e. using (8) and (9), using the same ranges of fitting domains. The results are reported in Fig. 6b. In this case, C_w is the initial slope of the fitting function $\hat{W}(\Delta\theta)$. As can be noted, the thermal capacitance is consistently evaluated independently by the interpolation domain. Moreover, almost the same thermal constant is estimated on the $\Delta\theta$ evolution, regardless of the calibration of $\Delta\theta_{st}$.

The thermal parameters obtained with [11] and with the proposed procedure are reported in Fig. 7, in blue and red dots respectively, while Tab. I presents their average values and dispersion. It can be easily noted that the parameters sensitivity in the original procedure is considerably greater than in the proposed one, which reduces the standard deviation of about one order of magnitude with respect to [11].

TABLE I
MEAN VALUE (μ) AND STANDARD DEVIATION (σ) OF THE ESTIMATED PARAMETER IN THE ORIGINAL AND PROPOSED PROCEDURE.

	μ		σ	
	[11]	Proposed	[11]	Proposed
C_w (p.u.)	1.220	0.859	0.222	0.021
τ_{eq} (p.u.)	1.389	1.091	0.299	0.051
R_{eq} (p.u.)	1.177	1.272	0.331	0.067

B. Validation over a Load Cycle

Finally, an application example is given in Fig. VI, where the parameters C_w and R_{th} extracted from the STTT were adopted for calibrating an advanced hotspot temperature observer, with the motor operating under a complex load cycle.

The temperature observer considers the thermal gradient of the machine, and it is meant to estimate the temperature of the

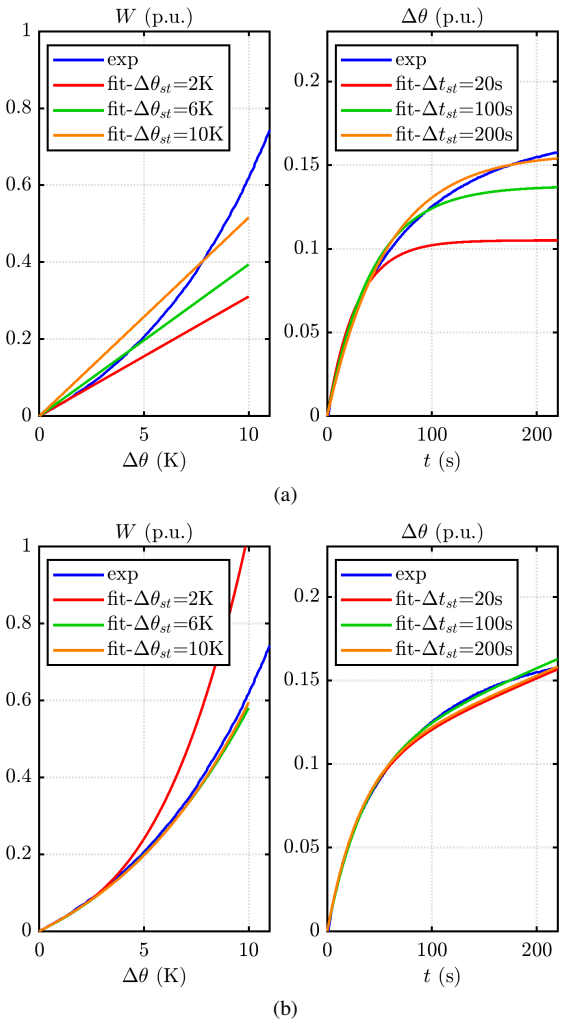

Fig. 6. Results of the STTT test. (a) Method in [11]: $W(\Delta\theta)$ interpolated with (4) and $\Delta\theta(t)$ interpolated with (5); (b) proposed solution: $W(\Delta\theta)$ interpolated with (8) and $\Delta\theta(t)$ interpolated with (9). The measured energy and temperature rise are interpolated on varying $\Delta\theta_{st}$and Δt_{st} respectively.

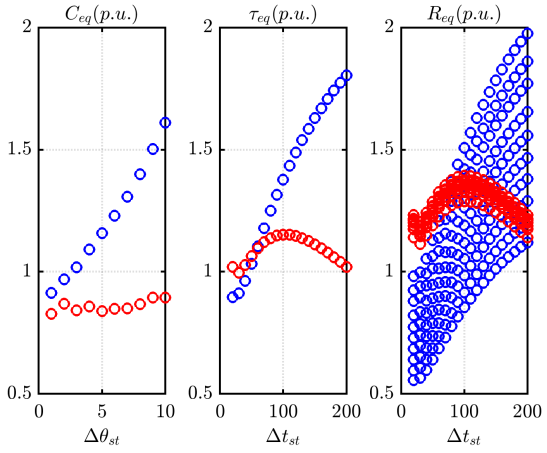

Fig. 7. Dispersion of the estimated parameters on varying $\Delta\theta_{st}$ and Δt_{st}. Blue: method in [11]; red: proposed analysis.

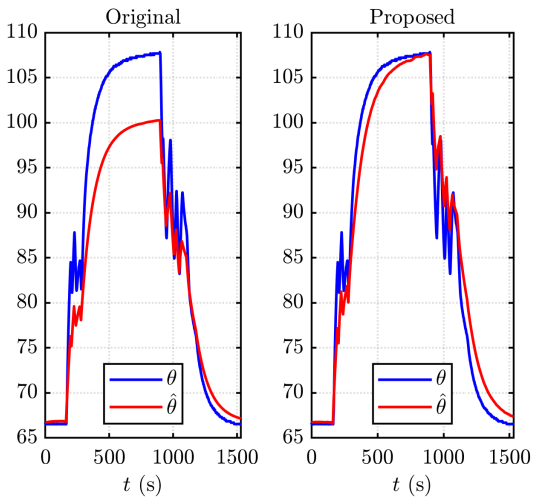

Fig. 8. Example of temperature prediction through a LPTN calibrated with [11] (left) and with the proposed analysis (right).

winding hotspot based on a thermistor placed in a colder point of the machine. The results in Fig. VI compare the temperature estimate obtained while calibrating the temperature observer based on [11] (left subplot) and with the proposed procedure (right subplot). As can be noted, the better calibration of the advanced LPTN permits a much more reliable temperature prediction.

VI. Conclusions

The STTT model permits to determine the thermal capacitance of the stator winding and the equivalent thermal resistance between the winding and the stator iron, that are key building blocks for an accurate LPTN transient thermal model of and AC machine. The thermal model enables the safe peak and continuous performance, and increases the reliability of the electric drive altogheter. This work proposed and validated an improved STTT testing procedure for high performance, liquid cooled motor drives. A novel experimental setup guarantees the thermal symmetry of the motor without requiring the access to the windings output terminals. Furthermore, the newly proposed 2nd order LPTN and post-processing method can accurately retrieve the winding thermal parameters independently from the domain of the thermal analysis, dropping the adiabatic hypothesis of previous methods. The proposed STTT approach is validated with experiments, demonstrating its accuracy and robustness.

Acknowledgment

The research has been conducted with the support of Power Electronics Innovation Center (PEIC) of Politecnico di Torino.

References

[1] N. Rivière, M. Stokmaier, and J. Goss, "An innovative multi-objective optimization approach for the multiphysics design of electrical machines," in *2020 IEEE Transportation Electrification Conference & Expo (ITEC)*, 2020, pp. 691–696.

[2] S. Li, Y. Li, W. Choi, and B. Sarlioglu, "High-Speed Electric Machines: Challenges and Design Considerations," *IEEE Transactions on Transportation Electrification*, vol. 2, no. 1, pp. 2–13, Mar. 2016.

[3] A. Boglietti, A. M. El-Refaie, O. Drubel, A. M. Omekanda, N. Bianchi, E. B. Agamloh, M. Popescu, A. Di Gerlando, and J. Borg Bartolo, "Electrical Machine Topologies: Hottest Topics in the Electrical Machine Research Community," *IEEE Industrial Electronics Magazine*, vol. 8, no. 2, pp. 18–30, Jun. 2014.

[4] R. Leuzzi and et Al., "Transient overload characteristics of pm-assisted synchronous reluctance machines, including sensorless control feasibility," *IEEE Transactions on Industry Applications*, vol. 55, no. 3, pp. 2637–2648, 2019.

[5] F. Momen, K. Rahman, and Y. Son, "Electrical propulsion system design of chevrolet bolt battery electric vehicle," *IEEE Transactions on Industry Applications*, vol. 55, no. 1, pp. 376–384, 2019.

[6] W. Jiang and T. M. Jahns, "Coupled electromagnetic–thermal analysis of electric machines including transient operation based on finite-element techniques," *IEEE Transactions on Industry Applications*, vol. 51, no. 2, pp. 1880–1889, 2015.

[7] A. Krings and C. Monissen, "Review and trends in electric traction motors for battery electric and hybrid vehicles," in *2020 International Conference on Electrical Machines (ICEM)*, vol. 1, 2020, pp. 1807–1813.

[8] A. Varatharajan, P. Pescetto, and G. Pellegrino, "Sensorless self-commissioning of synchronous reluctance machine with rotor self-locking mechanism," in *2019 IEEE Energy Conversion Congress and Exposition (ECCE)*, 2019, pp. 812–817.

[9] P. Pescetto and G. Pellegrino, "Determination of pm flux linkage based on minimum saliency tracking for pm-syr machines without rotor movement," *IEEE Transactions on Industry Applications*, vol. 56, no. 5, pp. 4924–4933, 2020.

[10] Y. Gai, M. Kimiabeigi, Y. Chuan Chong, J. D. Widmer, X. Deng, M. Popescu, J. Goss, D. A. Staton, and A. Steven, "Cooling of automotive traction motors: Schemes, examples, and computation methods," *IEEE Transactions on Industrial Electronics*, vol. 66, no. 3, pp. 1681–1692, 2019.

[11] A. Boglietti, E. Carpaneto, M. Cossale, and S. Vaschetto, "Stator-winding thermal models for short-time thermal transients: Definition and validation," *IEEE Transactions on Industrial Electronics*, vol. 63, no. 5, pp. 2713–2721, 2016.

[12] O. Wallscheid, "Thermal monitoring of electric motors: State-of-the-art review and future challenges," *IEEE Open Journal of Industry Applications*, vol. 2, pp. 204–223, 2021.

[13] N. Z. Popov, S. N. Vukosavic, and E. Levi, "Motor temperature monitoring based on impedance estimation at pwm frequencies," *IEEE Transactions on Energy Conversion*, 2014.

[14] C. Kral, A. Haumer, M. Haigis, H. Lang, and H. Kapeller, "Comparison of a cfd analysis and a thermal equivalent circuit model of a tefc induction machine with measurements," *IEEE Transactions on Energy Conversion*, vol. 24, no. 4, pp. 809–818, 2009.

[15] K. Bersch, S. Nuzzo, P. H. Connor, C. N. Eastwick, R. Rolston, and M. Galea, "Thermal and electromagnetic stator vent design optimisation for synchronous generators," *IEEE Transactions on Energy Conversion*, vol. 36, no. 1, pp. 207–217, 2021.

[16] M. C. Kulan and N. J. Baker, "Development of a thermal equivalent circuit to quantify the effect of thermal paste on heat flow through a permanent magnet alternator," *IEEE Transactions on Industry Applications*, vol. 55, no. 2, pp. 1261–1271, 2019.

[17] C. Sciascera, P. Giangrande, L. Papini, C. Gerada, and M. Galea, "Analytical thermal model for fast stator winding temperature prediction," *IEEE Transactions on Industrial Electronics*, vol. 64, no. 8, pp. 6116–6126, 2017.

[18] P. Pescetto, S. Ferrari, G. Pellegrino, E. Carpaneto, and A. Boglietti, "Winding thermal modeling and parameters identification for multithree phase machines based on short-time transient tests," *IEEE Transactions on Industry Applications*, vol. 56, no. 3, pp. 2472–2480, 2020.

[19] J. Goss, R. Wrobel, P. Mellor, and D. Staton, "The design of ac permanent magnet motors for electric vehicles: A design methodology," in *2013 International Electric Machines & Drives Conference*, 2013.

[20] P. Roy, A. J. Bourgault, M. Towhidi, P. Song, Z. Li, S. Mukundan, G. Rankin, and N. C. Kar, "An algorithm for effective design and performance investigation of active cooling system for required temperature and torque of pm traction motor," *IEEE Transactions on Magnetics*, vol. 57, no. 2, pp. 1–7, 2021.